ARTICLES
PUBLISHED ONLINE: 1 JUNE 2015 | DOI: 10.1038/NGEO2449
nature geoscience

Tug of war on summertime circulation between radiative forcing and sea surface warming

T. A. Shaw[1,2,3,4]* and A. Voigt[2]

During summertime, monsoons and subtropical anticyclones shape precipitation and regional circulation patterns across the globe. In state-of-the-art climate models, the average response of the Asian monsoon cyclone, Pacific ocean anticyclone and jet stream to global warming is weak and responses of different models are diverse. Here we use a suite of simulations with atmospheric general circulation models with prescribed sea surface temperatures to separate the circulation responses to direct radiative forcing and indirect sea surface temperature warming. We find that the two contributions oppose each other. Using idealized aquaplanet simulations, we show that the different circulation responses are directly connected to the opposite responses of land–sea thermal contrast to the two forcing components. This tug of war on the circulation response to global warming is analogous to the seasonal response to insolation, which involves opposite land–sea thermal contrasts and circulation patterns governed by quasi-equilibrium thermodynamics and stationary-wave dynamics. We conclude that it is important to distinguish weak circulation responses to global warming that arise owing to compensating effects that are robust and physically understood from those that are associated with genuine uncertainty. We note that compensation places fundamental limits on the detection and attribution of circulation responses to global warming.

The summertime circulation in the Northern Hemisphere is dominated by monsoon and subtropical anticyclone systems, which owe their existence to the distribution of continents and oceans. Each system involves monsoon precipitation, a low-level jet flowing into a monsoon cyclone over land that couples to oceanic anticyclones via stationary-wave dynamics[1–7]. Monsoon precipitation provides water to around one-half of the global population with the moisture source being advection by the low-level jet of water vapour evaporated from the tropical oceans. Subtropical anticyclones encompass 40% of the Earth's surface, they steer tropical cyclones towards North America and East Asia and bring low clouds and dry conditions to Mediterranean-type climate zones[5,8]. The most prominent summertime circulation feature is the Asian monsoon cyclone and low-level jet driven by diabatic heating[3–7]. The monsoon cyclone couples to the Pacific and Atlantic anticyclones and North American monsoon via a stationary zonal wavenumber-1 response to South and East Asian diabatic heating[3–5]. Coupling with the anticyclones is affected by the background flow, radiative cooling, low clouds and sea surface temperatures[5,6,8,9] (SSTs). The monsoon–anticyclone circulation exhibits a vertical baroclinic structure consistent with stationary waves in sverdrup balance[10]. The seasonal growth of monsoon–anticyclone systems coincides with pronounced changes in precipitation and circulation, including a northward shift of the intertropical convergence zone, local reversal of the trade winds and poleward shift of the extratropical jet stream[7,11].

Carbon dioxide (CO_2) concentrations are rising and are projected to increase further in the coming century. The response of monsoons and subtropical anticyclones to rising CO_2 concentrations will significantly influence regional climate during summertime. Understanding the physics underlying the response to global warming is important for ensuring confidence in future projections. The main conclusions of the Intergovernmental Panel on Climate Change (IPCC) Fifth Assessment Report[12] are that monsoon rainfall is likely to strengthen globally, the monsoon circulation is likely to weaken, onset dates are likely to occur earlier, and retreat dates are likely to occur later[13]. Previous authors have also shown that land–sea temperature contrasts will increase[14–16] and subtropical anticyclones will strengthen[17] in response to global warming. Intensification of anticyclones has been proposed as the cause of increased coastal ocean upwelling[18]. In the extratropics, the zonal-mean jet stream is predicted to shift poleward[19–22], yet this does not occur in the North Pacific Basin during summertime where there is a weak jet shift that is not robust across the models[22].

Here we show that the summertime circulation response to global warming in the Northern Hemisphere can be decomposed into components associated with direct CO_2 radiative forcing and indirect SST warming. These two components produce a tug of war involving opposite Asian monsoon cyclone, Pacific anticyclone and jet stream responses that can be understood using the seasonal circulation response to changes in solar insolation, quasi-equilibrium thermodynamics and stationary-wave dynamics. The response to direct CO_2 radiative forcing, increased solar insolation, and interannual variability in low-level winds over Asia involves positive land–sea sub-cloud equivalent potential temperature (θ_e) contrasts, low-level convergence around Asia, a stronger Asian monsoon cyclone and Pacific anticyclone, and a poleward shift of the Pacific jet stream. The response to SST warming and decreased solar insolation involves negative land–sea θ_e contrasts, low-level divergence around Asia, a weaker Asian monsoon cyclone and Pacific anticyclone and an equatorward jet shift. The opposite responses explain the weak multi-model-mean summertime circulation response to global warming in the Asia-Pacific region, including the weak shift of the Pacific jet stream.

Direct radiative forcing versus indirect SST warming

We assess the regional summertime (June, July and August) circulation response to global warming using output from state-of-the-art climate models participating in Coupled Model

[1]Department of the Geophysical Sciences, University of Chicago, Chicago, Illinois 60640, USA. [2]Lamont-Doherty Earth Observatory, Columbia University, New York, New York 100964, USA. [3]Department of Earth and Environmental Sciences, Columbia University, New York, New York 10027, USA. [4]Department of Applied Physics and Applied Mathematics, Columbia University, New York, New York 10027, USA. *e-mail: tas1@uchicago.edu

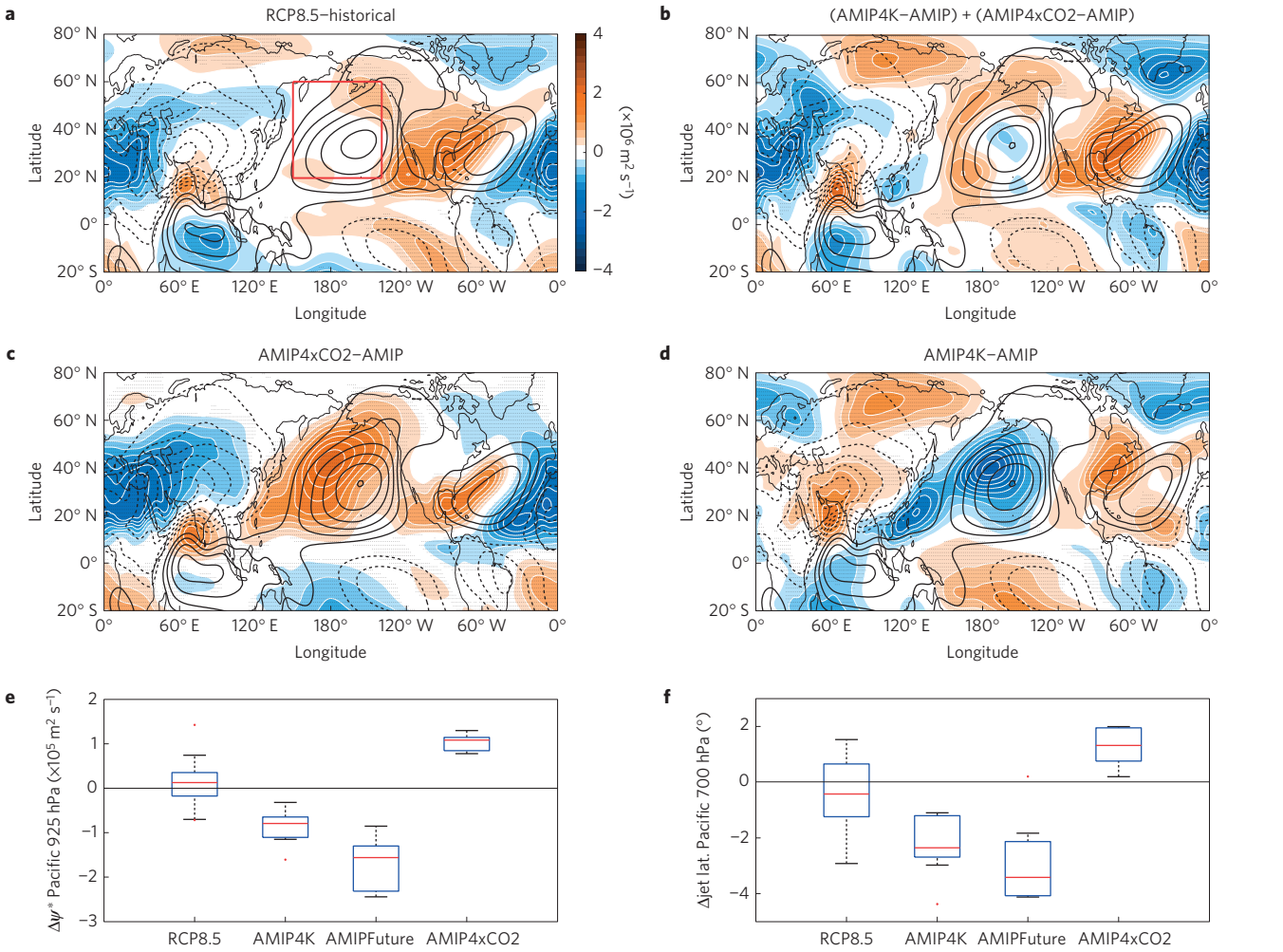

Figure 1 | Multi-model-mean summertime circulation response to global warming. a–d, Response of 925 hPa stationary eddy streamfunction (ψ^*, colour shading) relative to the historical period (**a**) and AMIP experiments (**b–d**). Colour scale in **a** applies to **a–d**. Contour interval for the black contours is 2.5×10^6 m^2 s^{-1}, negative values are dashed. Stippling indicates >80% model agreement on the sign of the response. **e**,**f**, Pacific response (red square in **a**) for 925 hPa stationary eddy streamfunction (**e**) and 700 hPa jet stream position (**f**) showing 25th–75th (blue box), 50th (red line), and 10th and 90th (black lines) percentiles.

Intercomparison Project phase 5 (CMIP5; ref. 23; see Methods and Supplementary Methods). A standard measure of the summertime circulation is the stationary eddy streamfunction[3–6,10,11] because summertime circulation features are related to the distribution of continents and oceans (monsoon cyclones over the continents and anticyclones over the oceans) and hence are largely fixed in space and time. Figure 1a shows the CMIP5 multi-model-mean low-level stationary eddy streamfunction response to the high-emission (Representative Concentration Pathway (RCP)8.5) IPCC scenario relative to the historical period. The longitudinally averaged eddy streamfunction amplitude is predicted to increase in agreement with CMIP3 models[17]; however, there are significant regional variations. Over North Africa there is an increase in strength with high confidence across the models (stippling indicates >80% model agreement); however, the Atlantic subtropical anticyclone shifts westward rather than strengthening in place. The response of the Asian monsoon cyclone and Pacific anticyclone is very weak and the models do not agree on the sign of the projected change.

The lack of consensus in the Asian monsoon cyclone and Pacific anticyclone response to global warming could be interpreted as lack of model skill and low confidence in the model projection. Here we show that the weak Asian monsoon cyclone and Pacific anticyclone response is the result of opposing responses to direct atmospheric radiative forcing and indirect SST warming. The opposing responses are revealed in idealized Atmosphere Model Intercomparison Project (AMIP) experiments in which SSTs are prescribed as opposed to computed with an ocean model (see Methods). The response to direct radiative forcing is quantified by quadrupling CO_2 while holding SSTs fixed (AMIP4xCO2). The indirect response to SST warming is quantified by increasing SST everywhere by 4 K (AMIP4K) or by imposing an SST pattern from the coupled atmosphere–ocean model response to increased CO_2 (AMIPFuture). Although the decomposition may seem artificial because CO_2 does not quadruple, the SST response is not uniform and there are other forcings, for example, aerosols and ozone, in RCP8.5, previous authors have successfully applied it to circulation trends[24,25], and the response of tropical precipitation[26] and Far East Asian (110°–170° E, 30°–70° N) land–sea temperature contrast[15,16] to global warming. Indeed, the combined stationary eddy streamfunction response to direct radiative forcing and 4 K SST warming agrees with the RCP8.5 response (compare Fig. 1b to Fig. 1a) in regions of robust (stippled) model response. Moreover, the combined AMIP response shows the same pattern of non-robustness (unstippled), including the western Pacific.

The AMIP experiments reveal oppositely signed Asian monsoon cyclone and Pacific anticyclone responses to direct radiative forcing

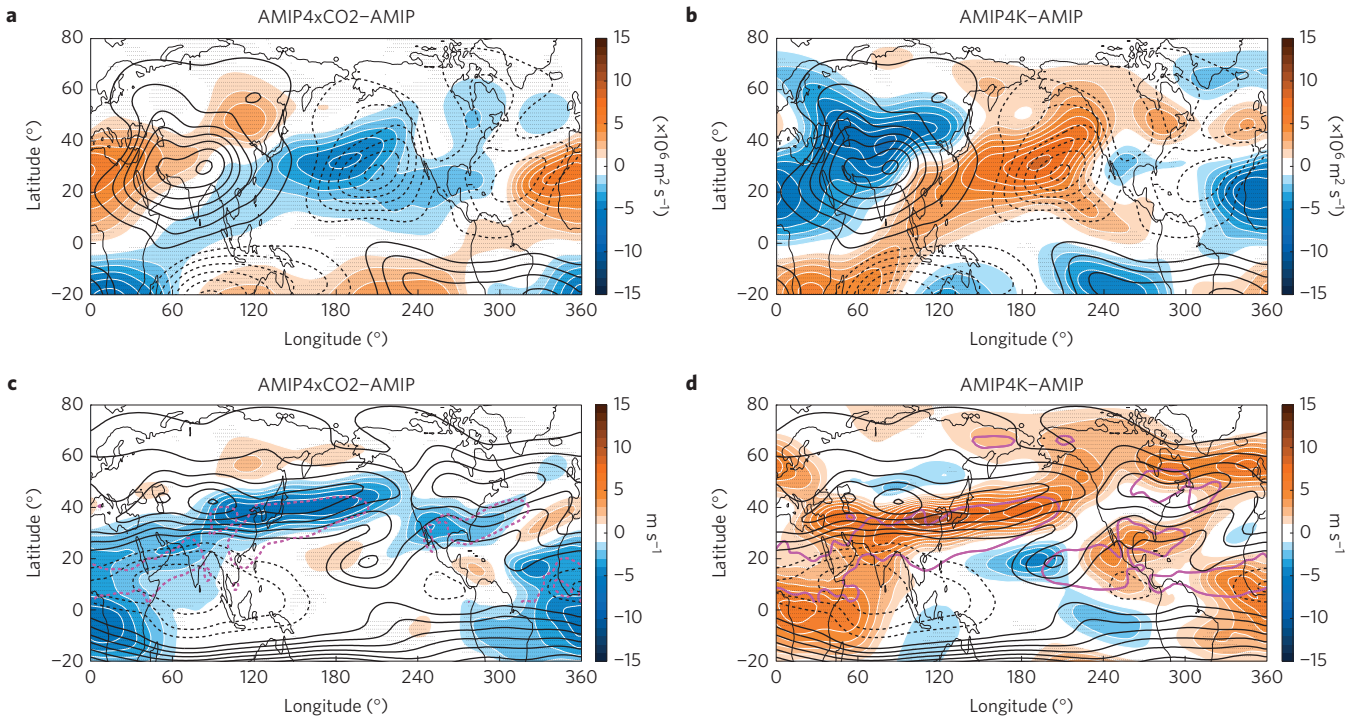

Figure 2 | Summertime circulation response in the upper troposphere. a–d, Response of 200 hPa stationary eddy streamfunction (**a**,**b**) and zonal wind (**c**,**d**) are shown by the colour shading, relative to AMIP (black contours). Contour interval for AMIP is 4.0×10^6 m^2 s^{-1} (**a**,**b**), 5.0 m s^{-1} (**c**,**d**). Negative values are dashed. Magenta contours indicate where the upper-level zonal wind response predicted from quasi-equilibrium (see Methods) is 5 m s^{-1} (solid) and −5 m s^{-1} (dashed). Stippling as in Fig. 1.

and indirect SST warming. Direct radiative forcing strengthens the Asian monsoon cyclone and Pacific anticyclone (Fig. 1c) whereas SST warming weakens them (Fig. 1d). Thus, the weak Asia-Pacific circulation response in the RCP8.5 scenario is the result of opposing responses, which largely cancel (Fig. 1b). The circulation over North Africa strengthens in response to direct radiative forcing and the Atlantic anticyclone shifts westward in response to direct radiative forcing and indirect SST warming.

The opposite Pacific anticyclone responses to direct radiative forcing and indirect SST warming (Fig. 1e) are consistent with opposite Pacific jet stream responses in the lower troposphere (Fig. 1f). In the upper troposphere, the stationary eddy streamfunction and jet stream responses extending from North Africa to the Pacific are also opposite, suggesting a vertically coupled stationary eddy response. Direct radiative forcing strengthens and shifts the eddy streamfunction westward (Fig. 2a) and the Pacific jet stream weakens and shifts poleward (Fig. 2c). The response to imposed SST warming is opposite (Fig. 2b,d). The opposite responses account for the weak shift of the Pacific jet stream in response to the RCP8.5 scenario[22]. The poleward shift of the Atlantic jet stream is dominated by indirect SST warming[27].

Understanding future regional circulation changes

Why do the Asian monsoon cyclone, Pacific anticyclone and jet stream exhibit opposite responses to direct radiative forcing and indirect SST warming? The opposite responses involve thermodynamic and dynamic mechanisms similar to those operating seasonally in response to changing solar insolation. In response to increased solar insolation, that is, July minus May, the Asian monsoon cyclone and Pacific anticyclone strengthen (Fig. 3a) and the Pacific jet stream shifts poleward. The monsoon cyclone represents a stationary-wave (rotational flow) response to low-level convergence[3–5] (inferred from vertical motion, Fig. 3c) around Asia (60°–120° E, 10°–40° N) co-located with increased sub-cloud θ_e and positive meridional θ_e gradient (magenta contour). There are also changes in vertical motion over the west Pacific ocean related to the SST seasonal cycle that affect the zonal-mean circulation. Asian monsoon precipitation is co-located with maximum θ_e seasonally and interannually[28,29] consistent with quasi-equilibrium theories of the tropical circulation[30–32]. Moisture converges into the region of large θ_e providing the moisture to sustain precipitation (Supplementary Fig. 1). The Asian monsoon cyclone is coupled to the Pacific and Atlantic anticyclones via the stationary zonal wavenumber-1 response to diabatic heating[3–5]. The response is localized in the ocean basins via the background flow and feedbacks involving radiative cooling, low clouds and SST coupling[5,6,8,9]. The poleward shift of the Pacific jet is partly due to subtropical stationary eddy momentum flux in the upper troposphere, which decelerates the zonal flow and shifts the critical layer for transient eddies poleward[11].

Similar thermodynamic and circulation patterns occur in response to direct radiative forcing from CO_2: the Asian monsoon cyclone and Pacific anticyclone strengthen (Fig. 1c), sub-cloud θ_e, its meridional gradient (magenta contour) and low-level convergence increase around Asia (60°–120° E, 10°–40° N, Fig. 3e), and the Pacific jet shifts poleward (Fig. 1e). Increased low-level convergence around Asia accounts for the westward shift of the upper tropospheric Tibetan anticyclone (Fig. 2a) via upper-level divergence and Rossby wave generation[33]. The sub-cloud θ_e response partly reflects the rapid adjustment to radiative forcing over land (for example, increased energy input and warming over land, decreased energy input over the fixed-SST ocean)[26,34] that promotes dynamical moisture flux convergence (Supplementary Fig. 1). The similarity of the circulation responses to direct CO_2 radiative forcing and increased insolation is consistent with both forcings producing a positive meridional θ_e gradient response around Asia (magenta contour, Fig. 3c,e). Interannual variations in South Asian monsoon winds involve a similar response (Supplementary Fig. 2a,b). Quasi-equilibrium theories predict that a positive land–sea θ_e contrast

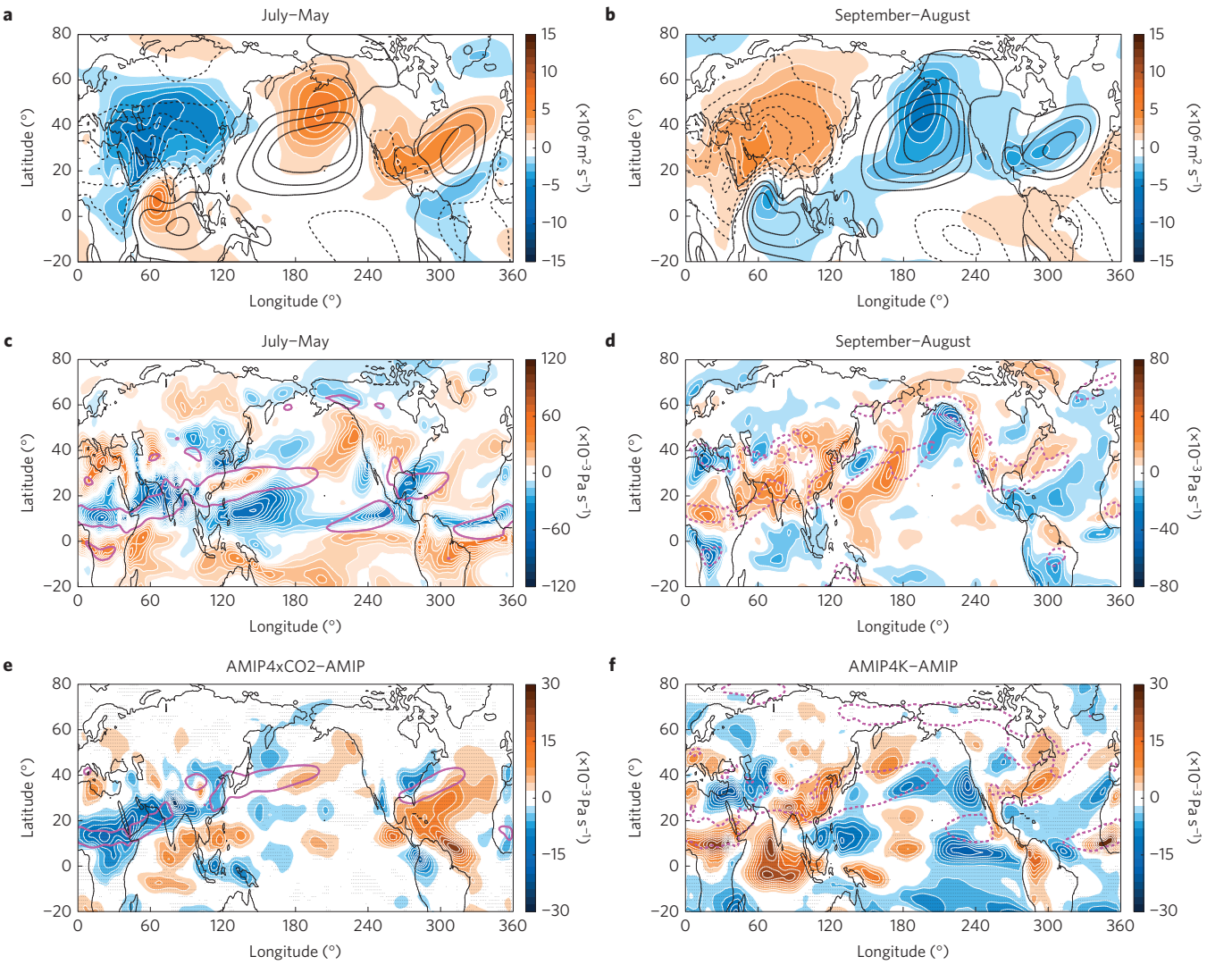

Figure 3 | Response to seasonal solar insolation versus global warming. a,**b**, Seasonal response of 925 hPa stationary eddy streamfunction (colour shading) relative to May (black, **a**) and August (black, **b**) from ERAinterim. Contour interval is 2.5×10^6 m^2 s^{-1} (black). Negative values are dashed. **c**–**f**, Response of 500 hPa vertical velocity in ERAinterim (**c**,**d**) and AMIP simulations (**e**,**f**). Stippling as in Fig. 1. Magenta contours indicate where the response of 925 hPa meridional θ_e gradient is 6×10^{-6} Km^{-1} (**c**), -4×10^{-6} Km^{-1} (**d**), 2×10^{-6} Km^{-1} (**e**) and -2×10^{-6} Km^{-1} (**f**). Note the different colour scales.

response will amplify the surface and upper-level eddy circulations, consistent with a vertical baroclinic structure[30]. The upper-level zonal wind predicted from quasi-equilibrium (see Methods) agrees well with the response to direct radiative forcing (magenta contour, Fig. 2c). Orography can also affect the thermal contrast around Asia and thereby the monsoon circulation[35].

Consistent with the similarity of the response to increased solar insolation and CO_2 radiative forcing, the response to decreased solar insolation is similar to imposed SST warming. In response to decreased insolation, that is, September minus August, the land cools faster than the ocean decreasing the meridional θ_e gradient (dashed magenta contour), there is low-level divergence around Asia (60°–120° E, 10°–40° N, Fig. 3d), the Asian monsoon cyclone and Pacific anticyclone weaken (Fig. 3b), and the Pacific jet shifts equatorward. Similar patterns occur in response to SST warming: there is low-level divergence and a negative meridional θ_e gradient around Asia (dashed magenta contour, Fig. 3f) consistent with increased θ_e over the ocean, the Asian monsoon cyclone and Pacific anticyclone weaken (Fig. 1d), and the Pacific jet shifts equatorward (Fig. 1f). Both forcings also involve dynamical moisture flux divergence around Asia (Supplementary Fig. 1). The similarity of the circulation response to decreased insolation and SST warming is consistent with both forcings producing a negative meridional θ_e gradient response around Asia (dashed magenta contour, Fig. 3d,f). Quasi-equilibrium theories predict that a negative land–sea θ_e contrast response will weaken the circulation[30]. The upper-level zonal wind predicted from quasi-equilibrium agrees well with the response to indirect SST warming (magenta contour, Fig. 2d). Interannual variations in East Asian monsoon winds produce a negative θ_e contrast, which weakens the Pacific anticyclone but does not significantly impact the Pacific jet (Supplementary Fig. 2c,d).

To test the explanation that opposite land–sea θ_e contrasts produce a tug of war on the Asian monsoon cyclone, Pacific anticyclone and jet stream we make use of idealized aquaplanet simulations (see Methods). The idealized simulations impose a monsoon cyclone–subtropical anticyclone circulation using zonally asymmetric SST patterns[11] (see Methods). When the θ_e gradient is increased by warming Asia (solid magenta contour, Fig. 4a,c), convergence and precipitation increase, the Asian monsoon cyclone and Pacific anticyclone strengthen, and the jet stream shifts

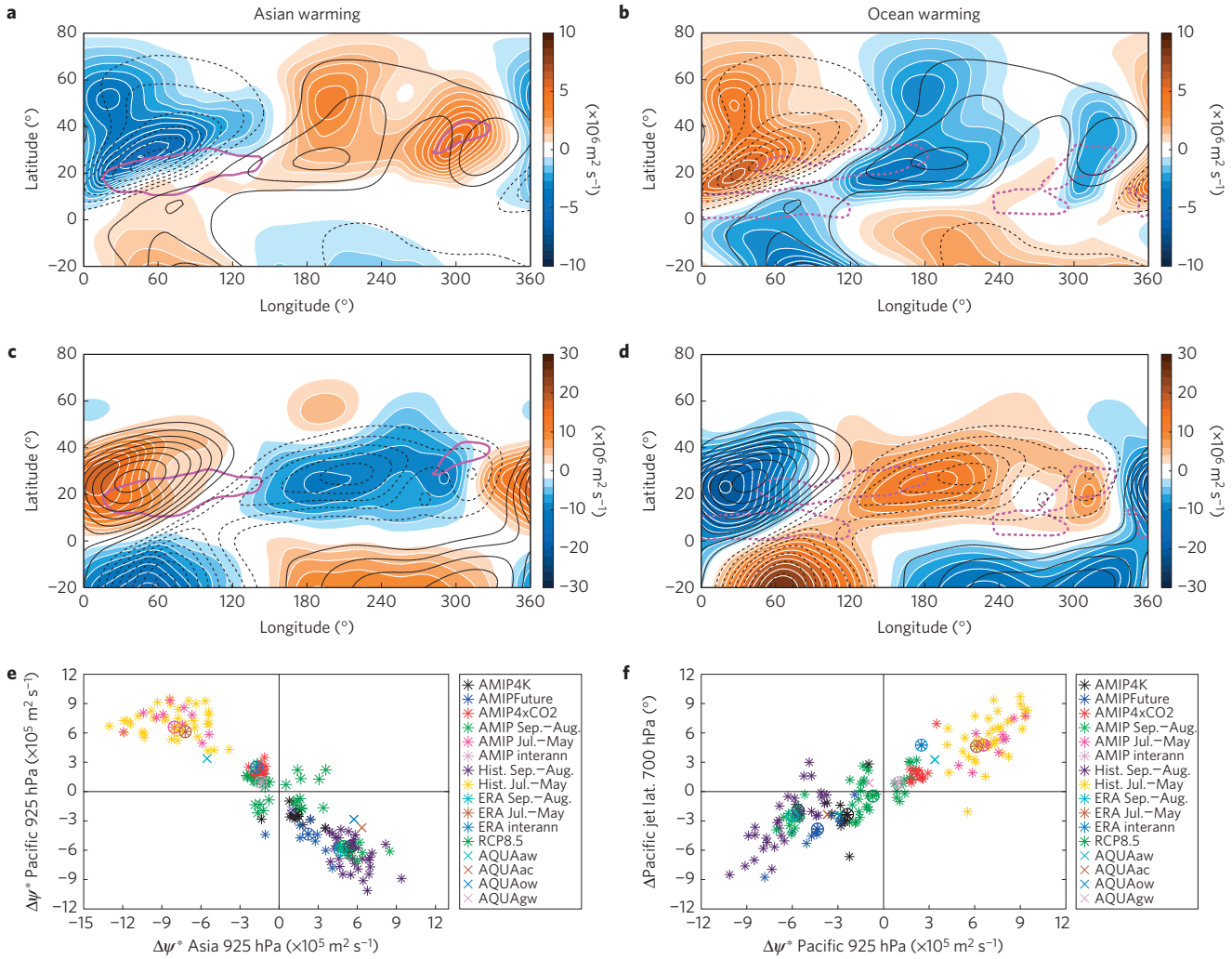

Figure 4 | Importance of land–sea contrasts. a–d, Aquaplanet model 925 hPa (**a**,**b**) and 200 hPa (**c**,**d**) stationary eddy streamfunction response (colour shading) relative to control (black). Contour interval for the control is 2.5×10^6 m^2 s^{-1} (**a**,**b**) and 6.0×10^6 m^2 s^{-1} (**c**,**d**). Thick magenta contours as in Fig. 3e,f. **e**, Local extrema (maximum or minimum) of 925 hPa stationary eddy streamfunction response in the North Pacific (130°–230° E, 35°–60° N) versus Asia (30°–110° E, 20°–40° N) for different forcings. **f**, Shift of 700 hPa Pacific jet stream versus extrema of North Pacific stationary eddy streamfunction response for different forcings. Stars represent individual models and circled stars represent multi-model mean or reanalysis.

poleward. In addition, the Atlantic anticyclone shifts westward consistent with the response to direct CO_2 forcing (Fig. 1c) and increased solar insolation (Fig. 3a). The aquaplanet results show that θ_e changes over the Pacific and Atlantic (magenta contour Fig. 3) occur in response to Asian changes. When the θ_e gradient is decreased by warming the ocean (dashed magenta contour, Fig. 4b,d), convergence and precipitation decrease over land, the monsoon cyclone and ocean anticyclone weaken, and the jet stream shifts equatorward. Similar patterns are seen in response to Asian cooling; however, the responses to uniform global warming, approximately uniform θ_e warming and $4xCO_2$ are all very weak (Supplementary Fig. 4). This confirms the importance of θ_e contrasts (driven either by local SST anomalies or land adjustment to increased CO_2) and their ability to produce a tug of war in state-of-the-art models. Indeed, the land–sea θ_e contrast response in the RCP8.5 scenario is weak and not robust in the Asia-Pacific region (Supplementary Fig. 5) consistent with the circulation response (Fig. 1a). The equality of θ_e over land and ocean has been used in theories of the land–ocean temperature contrast response to global warming[36].

The link between the Asian monsoon cyclone, Pacific anticyclone and jet stream is robust across model configuration (reanalysis, fully coupled atmosphere ocean, AMIP, and aquaplanet models) and timescales (seasonally, interannually, forced response to global warming, Fig. 4e,f). Thus, the tug of war on the monsoon, anticyclone and jet stream in response to global warming is analogous to that which occurs seasonally.

Our results show that circulation compensation occurs in response to opposite land–sea θ_e contrasts consistent with quasi-equilibrium predictions. In response to seasonal solar insolation, compensation occurs in the America-Atlantic region (Fig. 3a,b) consistent with opposite land–sea θ_e contrasts (Fig. 3c,d), which are influenced by Asia (Fig. 4a and Supplementary Fig. 4a). Compensation is also seen in the aquaplanet simulations, which do not have land (Supplementary Fig. 4c,e). Why does compensation not occur in the America-Atlantic region in response to global warming? Compensation does not occur partly because direct radiative forcing and indirect SST warming do not produce opposite θ_e responses in that region (Fig. 3e,f). The America-Atlantic response is fundamentally different for at least three reasons: in response to SST warming the largest θ_e changes do not occur next to subtropical land but instead in the tropical Atlantic (Fig. 3f), furthermore the largest subtropical convergence is over land (40°–60° N, 240°–270° E, Fig. 3f), and finally the America-Atlantic

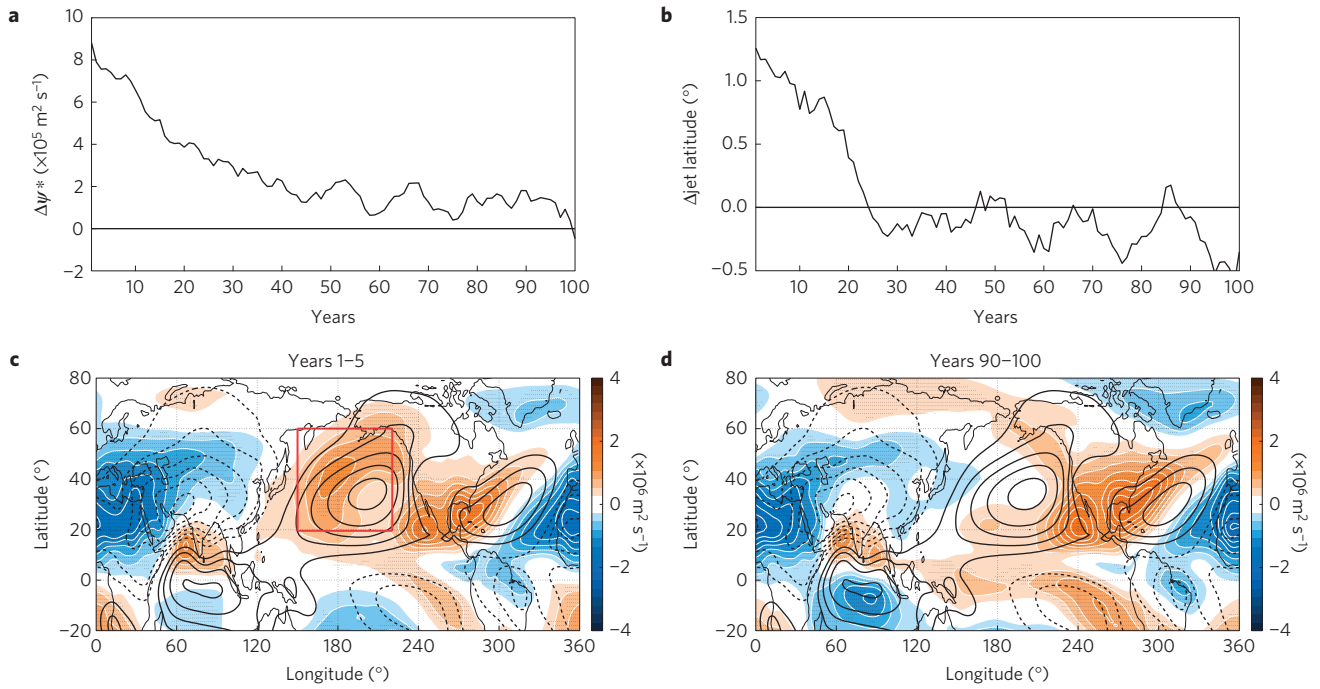

Figure 5 | Temporal evolution of the circulation tug of war. a,**b**, Transient evolution of the summertime (June–August) 925 hPa stationary eddy streamfunction (**a**) and 700 hPa jet stream position (**b**) in the Pacific (red square in **c**) in the abrupt4xCO2 simulation relative to the pre-industrial control simulation. **c**,**d**, Stationary eddy streamfunction response at 925 hPa with contouring and stippling as in Fig. 1.

region can be influenced by the Asian circulation (Fig. 4a and Supplementary Fig. 2a,b). Ultimately our results motivate future research into the role of local versus nonlocal effects.

Timescale of the tug of war

The circulation response to global warming has thus far been considered in equilibrium. Real-world climate change involves time-varying CO_2 changes and ocean warming (and never one but not the other). On what timescale does the circulation tug of war occur? In the seasonal cycle the tug of war occurs on monthly timescales reflecting both solar insolation and the different thermal inertias of land and ocean. The timescale of the response to CO_2 can be assessed using the CMIP5 coupled atmosphere–ocean model response to abrupt quadrupling of CO_2 (see Methods). In response to abrupt quadrupling of CO_2, the summertime stationary eddy streamfunction in the Pacific increases abruptly (Fig. 5a) and the pattern looks similar to the response to direct radiative forcing (compare Fig. 5c to Fig. 1c). Over decadal timescales the response weakens and converges to a weak response that agrees with RCP8.5 (compare Fig. 5d to Fig. 1a). Consistent with the Asia-Pacific circulation evolution, the Pacific jet stream shifts poleward initially and then subsequently equatorward converging to a weak response (Fig. 5b). The response timescale reflects a fast adjustment to CO_2 forcing and a subsequent adjustment involving SST warming. In reality, however, the CO_2 forcing increases gradually year-to-year, which makes a timescale separation in the circulation response difficult to detect and highlights the potential for compensation in the transient response to climate change.

We have shown that direct radiative forcing and indirect SST warming produce a tug of war on the summertime circulation response to global warming over the Asia-Pacific region. The tug of war has important implications for the jet stream, local weather, hurricane steering, coastal upwelling, low clouds over the Eastern Pacific and the Atlantic anticyclone. Our work demonstrates the importance of distinguishing weak projected circulation responses to global warming that arise because of genuine uncertainty and lack of model agreement from weak responses that arise owing to competing effects that are robust and physically understood. Situations involving weak circulation responses due to linearly additive, regionally competing effects are not uncommon. For example, the future Southern Hemisphere summertime circulation is expected to involve a tug of war between ozone recovery and greenhouse gas increases[37–39]. Arctic amplification and cooling of the extratropical lower stratosphere due to increased CO_2 produce opposite wintertime meridional temperature gradient responses that stand to move the Northern Hemisphere jet stream and storm tracks in opposite directions[40,41]. Finally, historical aerosol and CO_2 forcing produce opposite impacts on the Asian monsoon circulation[42,43]. In each case there is a strong seasonal dependence of the mechanisms involved in the tug of war that can be masked in an annual average. Confidence in model projections of regional circulation responses to global warming and the attribution and detection of those responses must account for compensating signals.

Methods

Methods and any associated references are available in the online version of the paper.

Received 18 November 2014; accepted 23 April 2015; published online 1 June 2015

References

1. Webster, P. J. Response of the tropical atmosphere to local, steady forcing. *Mon. Weath. Rev.* **100,** 518–541 (1972).
2. Gill, A. E. Some simple solutions for heat-induced tropical circulation. *Q. J. R. Meteorol. Soc.* **106,** 447–462 (1980).
3. Ting, M. Maintenance of the Northern Summer stationary waves in a GCM. *J. Atmos. Sci.* **51,** 3286–3308 (1994).
4. Wang, H. & Ting, M. Seasonal cycle of the climatological stationary waves in the NCEP-NCAR reanalysis. *J. Atmos. Sci.* **56,** 3892–3919 (1999).
5. Rodwell, M. J. & Hoskins, B. J. Subtropical anticyclones and summer monsoons. *J. Clim.* **14,** 3192–3211 (2001).
6. Chen, P., Hoerling, M. P. & Dole, R. The origin of subtropical anticyclones. *J. Atmos. Sci.* **58,** 1827–1835 (2001).

7. Webster, P. & Fasullo, J. in *Encyclopedia of Atmospheric Sciences* (eds Holton, J. R., Curry, J. A. & Pyle, J. A.) 1370–1391 (Academic Press, 2003).
8. Seager, R. *et al.* Air–sea interactions and the seasonal cycle of the subtropical anticyclones. *J. Clim.* **16,** 1948–1966 (2003).
9. Liu, Y., Wu, G. & Ren, R. Relationship between the subtropical anticyclone and diabatic heating. *J. Clim.* **17,** 682–698 (2004).
10. Chen, T-C. Characteristics of summer stationary waves in the Northern Hemisphere. *J. Clim.* **23,** 4489–4507 (2010).
11. Shaw, T. A. On the role of planetary-scale waves in the abrupt seasonal transition of the Northern Hemisphere general circulation. *J. Atmos. Sci.* **71,** 1724–1746 (2014).
12. IPCC *Climate Change 2013: The Physical Science Basis* (eds Stocker, T. F. *et al.*) (Cambridge Univ. Press, 2013).
13. Christiansen, J. H. *et al.* in *Climate Change 2013: The Physical Science Basis* (eds Stocker, T. F. *et al.*) Ch. 14, 1217–1308 (IPCC, Cambridge Univ. Press, 2013).
14. Manabe, S., Stouffer, R. J., Spelman, M. K. & Bryan, K. Transient responses of a coupled ocean-atmosphere model to gradual changes of atmospheric CO_2. Part I: Annual mean response. *J. Clim.* **4,** 785–818 (1991).
15. Kamae, Y., Watanabe, M., Kimoto, M. & Shiogama, H. Summertime land–sea thermal contrast and atmospheric circulation over East Asia in a warming climate—Part I: Past changes and future projections. *Clim. Dynam.* **43,** 2553–2568 (2014).
16. Kamae, Y., Watanabe, M., Kimoto, M. & Shiogama, H. Summertime land–sea thermal contrast and atmospheric circulation over East Asia in a warming climate—Part II: Importance of CO_2-induced continental warming. *Clim. Dynam.* **43,** 2569–2583 (2014).
17. Li, W., Li, L., Ting, M. & Liu, Y. Intensification of the Northern Hemisphere subtropical highs in a warming climate. *Nature Geosci.* **5,** 830–834 (2012).
18. Bakun, A. Global climate change and the intensification of coastal ocean upwelling. *Science* **247,** 198–201 (1990).
19. Yin, J. H. A consistent poleward shift of the storm tracks in simulations of 21st century climate. *Geophys. Res. Lett.* **32,** L18701 (2005).
20. Lorenz, D. J. & DeWeaver, E. Tropopause height and zonal wind response to global warming in the IPCC scenario integrations. *J. Geophys. Res.* **112,** D10119 (2007).
21. Barnes, E. A. & Polvani, L. M. Response of the midlatitude jets, and their variability, to increased greenhouse gases in the CMIP5 models. *J. Clim.* **26,** 7117–7135 (2013).
22. Simpson, I. R., Shaw, T. A. & Seager, R. A diagnosis of the seasonally and longitudinally varying mid-latitude circulation response to global warming. *J. Atmos. Sci.* **71,** 2489–2515 (2014).
23. Taylor, K. E., Stouffer, R. J. & Meehl, G. A. An overview of CMIP5 and the experiment design. *Bull. Am. Meteorol. Soc.* **93,** 485–498 (2012).
24. Deser, C. & Phillips, A. S. Atmospheric circulation trends, 1950–2000: The relative roles of sea surface temperature forcing and direct atmospheric radiative forcing. *J. Clim.* **22,** 396–413 (2009).
25. Li, H., Dai, A., Zhou, T. & Lu, J. Responses of East Asian summer monsoon to historical SST and atmospheric forcing during 1950–2000. *Clim. Dynam.* **34,** 501–514 (2010).
26. Bony, S. *et al.* Robust direct effect of carbon dioxide on tropical circulation and regional precipitation. *Nature Geosci.* **6,** 447–451 (2013).
27. Grise, K. M. & Polvani, L. M. The atmospheric circulation response to increased CO_2: The relative roles of sea surface temperature forcing and direct atmospheric radiative forcing. *Geophys. Res. Lett.* **41,** 6863–6871 (2014).
28. Nie, X., Boos, W. R. & Kuang, Z. Observational evidence of a quasi-equilibrium view of monsoons. *J. Clim.* **23,** 4416–4428 (2010).
29. Hurley, J. V. & Boos, W. R. Interannual variability of monsoon precipitation and local subcloud equivalent potential temperature. *J. Clim.* **26,** 9507–9527 (2013).
30. Emanuel, K. A. On thermally direct circulation in moist atmospheres. *J. Atmos. Sci.* **52,** 1529–1534 (1995).
31. Lindzen, R. S. & Nigam, S. On the role of sea surface temperature gradients in forcing winds and convergence in the tropics. *J. Atmos. Sci.* **44,** 2418–2436 (1985).
32. Prive, N. & Plumb, A. Monsoon dynamics with interactive forcing. Part I: Axisymmetric studies. *J. Atmos. Sci.* **64,** 1417–1430.
33. Sardeshmukh, P. D. & Hoskins, B. J. The generation of global rotational flow by steady idealized tropical divergence. *J. Atmos. Sci.* **45,** 1228–1251 (1988).
34. Allen, M. R. & Ingram, W. J. Constraints on future changes in climate and the hydrological cycle. *Nature* **419,** 224–232 (2002).
35. Ma, D., Boos, W. R. & Kuang, Z. Effects of orography and surface heat fluxes on the South Asian Summer Monsoon. *J. Clim.* **27,** 6647–6659 (2014).
36. Byrne, M. & O'Gorman, P. Land–ocean warming contrast over a wide range of climates: Convective quasi-equilibrium theory and idealized simulations. *J. Clim.* **26,** 4000–4016 (2013).
37. McLandress, C. *et al.* Separating the dynamical effects of climate change and ozone depletion. Part II: Southern Hemisphere troposphere. *J. Clim.* **24,** 1850–1868 (2011).
38. Polvani, L. M., Waugh, D. W., Correa, G. & Son, S-W. Stratospheric ozone depletion: The main driver of twentieth-century atmospheric circulation changes in the Southern Hemisphere. *J. Clim.* **24,** 795–812 (2011).
39. Perlwitz, J. Tug of war on the jet stream. *Nature Clim. Change* **1,** 29–31 (2012).
40. Held, I. M. Large-scale dynamics and global warming. *Bull. Am. Meteorol. Soc.* **74,** 228–241 (1993).
41. Butler, A. H., Thompson, D. W. J. & Heikes, R. The steady-state atmospheric circulation response to climate change-like thermal forcings in a simple general circulation model. *J. Clim.* **23,** 3474–3496 (2010).
42. Bollasina, M. A., Ming, Y. & Ramaswamy, V. Anthropogenic aerosols and the weakening of the South Asian Monsoon. *Science* **334,** 502–505 (2011).
43. Li, X., Ting, M., Li, C. & Henderson, N. Mechanisms of Asian summer monsoon changes in response to anthropogenic forcing in CMIP5 models. *J. Clim.* http://dx.doi.org/10.1175/JCLI-D-14-00559.1 (2015).

Acknowledgements

T.A.S. and A.V. are supported by the David and Lucile Packard Foundation. T.A.S. acknowledges support from the National Science Foundation (Grant AGS-125520). We thank I. Simpson, R. Seager, M. Ting and A. Sobel for helpful discussions and N. Henderson and H. Liu for help downloading the CMIP5 data. We acknowledge the World Climate Research Programme's Working Group on Coupled Modelling, which is responsible for CMIP, and we thank the climate modelling groups (listed in the Supplementary Methods) for producing and making available their model output. For CMIP the US Department of Energy's Program for Climate Model Diagnosis and Intercomparison provides coordinating support and led development of software infrastructure in partnership with the Global Organization for Earth System Science Portals.

Author contributions

T.A.S. designed the study, performed the analysis and wrote the manuscript. A.V. and T.A.S. performed the aquaplanet model simulations. Both authors discussed and interpreted the results and edited the manuscript.

Additional information

Supplementary information is available in the online version of the paper. Reprints and permissions information is available online at www.nature.com/reprints. Correspondence and requests for materials should be addressed to T.A.S.

Competing financial interests

The authors declare no competing financial interests.

Methods

CMIP5 simulations. We used Coupled Model Intercomparison Project phase 5 (CMIP5) model simulations (see Supplementary Table 1). In all cases monthly data were used, the data were interpolated onto a common grid based on the ERA-Interim reanalysis data, and missing values were filled using the ncl poisson_grid_fill routine before averaging. The CMIP5 data used in this paper are available at http://cmip-pcmdi.llnl.gov/cmip5/data_portal.html.

For the historical and RCP8.5 scenarios the response to global warming is defined as the difference between the 2080 to 2099 period from the RCP8.5 simulation and the 1986 to 2005 period from the historical simulation following ref. 13. The standard AMIP simulation is run with historical SSTs and historical anthropogenic forcing from 1979 to 2008. Two additional experiments are performed to mimic different aspects of global warming. The AMIP4xCO2 simulations involve a quadrupling of the CO_2 concentration with the same historical SSTs (no change in SST). Complementary simulations involve increasing historical SSTs by 4 K everywhere with fixed historical CO_2 concentration (AMIP4K). Finally, AMIPFuture involves imposing the end-of-century SST response to the A1B scenario from CMIP3 models. The atmospheric response to the imposed forcing (AMIP4xCO2, AMIP4K or AMIPFuture) is quantified by the difference from the AMIP simulation. The response to abrupt quadrupling of CO_2 concentration is assessed from the 100-year abrupt4xCO2 simulations relative to the piControl simulations.

The vertical velocity and meridional θ_e gradient responses were smoothed isotropically in the spectral domain with coefficients $n=21$, $r=1$ following ref. 44.

Moisture budget. The vertically integrated moisture budget calculation follows the procedure described in ref. 45. The vertical integration is performed on 17 pressure levels.

ERA-Interim data. Daily data from 1979 to 2012 from the European Centre for Medium Range Weather Forecasting ERA-Interim reanalysis data set[46] were used in this study. The data can be accessed at http://apps.ecmwf.int/datasets/data/interim-full-daily.

Interannual variability. Interannual variability of the summertime circulation from 1979 to 2012 is assessed by regressing 925 hPa stationary eddy streamfunction and 700 hPa zonal wind onto the June South Asian monsoon index and the August East Asian monsoon index[47]. The indices represent interannual variability of the 850 hPa wind averaged over South Asia (35°–70° E, 5°–25° N) and East Asia (110°–140° E, 5°–40° N).

Zonal wind from quasi-equilibrium thermodynamics. Assuming quasi-radiative–convective equilibrium[30], the horizontal winds at the tropopause ($\mathbf{v}_T$) and at the surface ($\mathbf{v}_s$) are predicted to be

$$\mathbf{v}_T = \frac{(T_s - T_t)}{2\Omega \sin\phi}\mathbf{k} \times \nabla_p[c_p \ln(\theta_e^*)]$$

$$\mathbf{v}_s = \frac{(T_s - T_t)}{2\Omega \sin\phi}\mathbf{k} \times \nabla_p[c_p(\ln(\theta_{e_{crit}}) - \ln(\theta_e^*))]$$

where T_s and T_t are the surface and tropopause temperature, respectively, $\mathbf{\Omega}$ is Earth's rotation rate, c_p is the specific heat at constant pressure, θ_e^* is the sub-cloud θ_e and $\theta_{e_{crit}}$ is its critical value. The upper-level zonal wind in the Northern Hemisphere inferred from the quasi-equilibrium relationship is shown in Fig. 2c,d (magenta contours). The θ_e term dominates the wind response rather than the temperature difference term.

Aquaplanet model simulations. Aquaplanet model experiments were performed with the Max Planck Institute Earth System Model (MPI-ESM-LR) model[48]. In all cases a background SST is imposed as the 'Qobs' distribution[49] with the SST maximum shifted to 10° N following ref. 11 (Supplementary Fig. 3a). Zonally asymmetric SST patterns are imposed to mimic the monsoon–anticyclone circulation over the Asia-Pacific 0°–240° E and North America-Atlantic 240°–360° E regions (see Supplementary Fig. 3b). The model response to different forcings, for example, Asian warming (AQUAaw), ocean warming (AQUAow), Asian cooling (AQUAac), global warming (AQUAgw), uniform θ_e warming, is assessed using different combinations of SST patterns shown in Supplementary Fig. 4. Approximately uniform θ_e warming is achieved by imposing an SST using the following formula:

$$\delta\theta_e \approx \delta(\mathrm{SST}) + 0.07\delta(\mathrm{SST})L_v q_{cntl}/c_p$$

where q_{cntl} is the specific humidity in the control climate, L_v is the latent heat of vaporization, and c_p is the specific heat at constant pressure, which assumes humidity increases following the Clausius–Clapeyron relationship (~7% K^{-1}). Each simulation is run for 10 years. The simulation data are available from T.A.S. on request.

Code availability. The code used to generate the aquaplanet model experiments can be accessed at http://www.mpimet.mpg.de/en/science/models/model-distribution.html.

References

44. Sardeshmukh, P. D. & Hoskins, B. J. Spatial smoothing on the sphere. *Mon. Weath. Rev.* **112,** 2524–2529 (1984).
45. Seager, R. & Henderson, N. Diagnostic computation of moisture budgets in the ERA-Interim reanalysis with reference to analysis of CMIP-archived atmospheric model data. *J. Clim.* **26,** 7876–7901 (2013).
46. Dee, D. P. *et al.* The ERA-Interim reanalysis: Configuration and performance of the data assimilation system. *Q. J. R. Meteorol. Soc.* **137,** 553–597 (2011).
47. Li, J. P. & Zeng, Q. C. A unified monsoon index. *Geophys. Res. Lett.* **29,** 1151–1154 (2002).
48. Stevens, B. *et al.* Atmospheric component of the MPI-M Earth System Model: ECHAM6. *J. Adv. Model. Earth Syst.* **5,** 146–172 (2013).
49. Neale, R. & Hoskins, B. J. A standard test for AGCMs including their physical parameterizations. Part I: The proposal. *Atmos. Sci. Lett.* **1,** 101–107 (2001).